https://doi.org/10.48047/AFJBS.6.15.2024.7808-7823

African Journal of Biological Sciences

Journal homepage: http://www.afjbs.com

Research Paper Open Access

Synthesis and characterization of WO_3-few layer graphene nanocomposite for antibacterial and anticancer applications

M. Muniyalakshmi[a,f], D. Thilaga Sundari [b,f], C. Anantha Prabhu[c,f], R. Sarika[d], D. Silambarasan[*e,f], V. Prasanna Venkatesh[g],

[a]Research Scholar (19121072132009), PG and Research Department of Physics, The M.D.T. Hindu College, Tirunelveli - 627010, Tamil Nadu, India.

[b]Research Scholar (19231072132008), PG and Research Department of Physics, The M.D.T. Hindu College, Tirunelveli - 627010, Tamil Nadu, India.

[c]Research Scholar (21211072131001), PG and Research Department of Physics, The M.D.T. Hindu College, Tirunelveli - 627010, Tamil Nadu, India.

[d]Assistant Professor, Department of Chemistry, Fatima College (Autonomous), Madurai - 625018, Tamil Nadu, India.

[e]Assistant Professor, PG and Research Department of Physics, The M.D.T. Hindu College, Tirunelveli - 627010, Tamil Nadu, India.

[f]Affiliated to Manonmaniam Sundaranar University, Abishekapatti, Tirunelveli - 627012, Tamil Nadu, India.

[g] Assistant Professor, Department of Physics, Velammal College of Engineering and Technology, Madurai - 625009, Tamil Nadu, India.

(*Corresponding author email id: carbonlabmdt@gmail.com, silambarasan@mdthinducollege.org)

Volume 6, Issue 15, Aug 2024

Received: 15 July 2024

Accepted: 05 Aug 2024

Published: 25 Aug 2024

doi: 10.48047/AFJBS.6.15.2024.7808-7823

Abstract

In the present work, Tungsten trioxide nanoparticles (WO_3 NPs) are synthesized via precipitation, while few layer graphene (FLG) and WO_3-FLG nanocomposite (NC) are synthesised through ultra-sonication technique. XRD confirmed the existence of WO_3 and identified its crystal structure, as well as the phase composition of WO_3-FLG NC. SEM results support the morphology of FLG and the presence of WO_3 NPs on FLG. Raman analysis verified the presence of various vibrational modes in both samples. WO_3 and WO_3-FLG NC are evaluated for bacterial inactivation on S. aureus, E. coli strains and cytotoxicity influence on breast cancer cells. The observed results suggested that WO_3-FLG NC exhibit significant antibacterial and anticancer activities.

Keywords: Tungsten trioxide; Few layer graphene; Nanocomposite; Antibacterial; Anticancer activity.

1. Introduction

In recent years, nanotechnology has made great progress in producing innovative materials for novel applications. Tungsten trioxide (WO_3) is a versatile and widely studied transition metal oxide known for its unique chemical, optical, and electronic properties. it has a wide range of applications in various fields, including photo catalysis, energy storage, gas sensing, electrochromic devices, and environmental remediation, such as pollutant degradation and water disinfection, antibacterial and anticancer treatments by generating reactive oxygen species (ROS) that can break down harmful compounds or kill microorganisms [1–7]. Few layer graphene (FLG) is a form of graphene, consisting of a small number of graphene sheets stacked together, which retains the extraordinary electrical, mechanical, and thermal properties of graphene. It provides a high surface area, excellent electrical conductivity, and biocompatibility [8–10].

Combining WO_3 and FLG, the nanocomposite benefits from the complementary properties of both materials due to the synergistic effect. The FLG enhances the electron mobility of WO_3 by reducing electron-hole recombination, thus increasing the efficiency of photocatalytic reactions. This leads to better performance in generating ROS for applications such as antibacterial and anticancer treatments. The mechanical strength and flexibility of FLG also improve the stability and durability of the composite, making it more suitable for long term use. Although many researchers have reported on composites constructed from WO_3 and graphene derivatives, there is limited literature available on WO_3-FLG NC for antibacterial and anticancer applications [11-13]. Antibacterial activity of WO_3-GO NCs on E. coli and P. aeruginosa was tested by Muzaffar *et al.* [11]. WO_3-GO NCs was examined to inspect inactivation of B. subtilis and E. coli [7]. Ahmed *et al.* [12] successfully treated B. subtilis and P. aeruginosa microorganisms with WO_3-rGO composite. Jeevitha *et al.* [7] explored the anticancer efficacy of WO_3-GO nanocomposites using lung cancer cells. Alaizeri *et al.* [13] emphasized the deadly behavior of WO_3 and WO_3-rGO NCs on colorectal cancer cells (HCT116) and lung cancer cells (A549).

In this study, WO_3 NPs are synthesized by precipitation and FLG, WO_3-FLG NC are synthesised through ultra-sonication techniques. The antibacterial and anticancer properties of synthesized WO_3 and WO_3-FLG NC have been revealed.

2. Experimental

2.1 Materials and Methods

Graphite powder from LOBA, sodium tungstate from SRL, hydrochloric acid, ethanol and distilled water was used throughout the synthesis process. The precipitation method is an effortless process for producing WO_3 NPs [14]. Sodium tungstate dihydrate ($Na_2WO_4.2H_2O$, 3.28 g) was dissolved in 75 ml of distilled water and stirred for 30 minutes to form a homogeneous solution. The initial pH of the solution was approximately 8. Concentrated HCl was then gradually added during 2 hours of stirring, lowering the pH to approximately 2. After settling overnight, the precipitate was centrifuged and rinsed with distilled water and ethanol to remove impurities and attain a neutral pH (~7). The washed precipitate was dried at 120°C for 3 hours, followed by annealing at 450°C for another 3 hours to yield WO_3 NPs. The ultra-sonication method is a simple procedure used to synthesis few layer graphene [15]. Initially, 100 mg of graphite powder was dispersed in 100 ml of O-DCB and ultra-sonicated for 8 hours. As sonication progressed, the sample gradually transformed from light grey to a black dispersion. To avoid water heating, the water in the sonicate bath was changed on a frequent basis. After being undisturbed for two days, the precipitate was centrifuged at 3000 rpm for 20 minutes. Following centrifugation, undissolved graphitic layers were settled at the bottom of the solution. The top portion of the supernatant, consisting of a uniform exfoliated graphene dispersion, was carefully collected. WO_3-FLG (100mg) NC was produced using the ultra-sonication technique [16]. 1g of WO_3 was sonicated with 10 ml of distilled water and 10 ml of ethanol for 2 hours. Following that, 100 mg of the previously obtained exfoliated graphene dispersion (FLG) was gradually added to this solution while continuing the sonication. The WO_3-FLG NC was produced by sonicating the mixture for an additional 4 hours and drying it in an oven at 60°C for 6 hours.

2.2 Preparation of Antibacterial assay

WO_3 and WO_3-FLG NC have been examined for antibacterial effectiveness on S. aureus and E. coli cultures employing the agar well diffusion method. The bacterial cultures and distilled water was introduced into a nutrient agar medium under sterile conditions. Next, 100 µl of the cultivated bacteria was evenly distributed on separate plates containing WO_3 and WO_3-FLG NC with different concentrations, and the plates were incubated at 37°C for 24 hours. Following incubation, the zones of inhibition are measured in millimeters [17].

2.3 Preparation of MTT assay

The anticancer effectiveness of WO_3 and WO_3-FLG NC was verified using the breast cancer cell line MDA-MB-231, which was grown in 96 well plates according to the technique described in previous research work [18]. In short, each well contained 100 µl of grown culture (~10,000 cells) and 10 to 100 µl of WO_3 and WO_3-FLG NC, individually. The plates were incubated at 37℃ in a 5% CO_2 environment for 24 hours. After incubation, the sample solutions were removed and 100 µl of MTT solution (5 mg/10 ml in phosphate-buffered saline) were added to each well. The plates were incubated for another 4 hours at 37°C in a 5% CO_2 environment. Following that, the growth inhibition values were measured.

2.4 Apoptosis AO-EB (Acridine Orange/Ethidium Bromide) Analysis

Dual AO-EB fluorescence staining was employed to evaluate cell apoptosis induced by WO_3 and WO_3-FLG NC. In 24 well plates, cancer cells (2000 cells/well) were treated with WO_3 and WO_3-FLG NC (IC_{50} conc.). Plates were incubated at 37℃ for 24 hours. Following incubation, each well was applied 10 µl of a staining solution with 100 µg/ml of AO and with 100 µg/ml of EB. The cells were inspected under a fluorescence microscope, and photographs were taken to distinguish between live cells and dead cells [19].

2.5 Instrumentation

XRD spectra were obtained using a Bruker Axis D2 Phaser with CuKα radiation (λ = 1.5406 Å). SEM was performed with a Japanese JEOL JEM 2100 microscope. Raman spectra were acquired using an EZ Raman spectrometer. Antibacterial and anticancer investigations were conducted at the Biome Live Analytical Centre. Fluorescence imaging was accomplished using a Japanese Olympus CKX-53 microscope.

3. Results and discussion

3.1 X-Ray Diffraction (XRD)

The XRD spectra of FLG, WO_3 and WO_3-FLG NC are shown in Figure 1. The diffraction pattern of FLG (Fig. 1(a)) shows distinct peaks at 26.4 and 54.2º, which correspond to the (002) and (100) planes, respectively. The literature confirms the graphitic nature of FLG [20, 21]. The number of layers (N) of the synthesized FLG was calculated using Scherer formula [8, 22], based on peak position (002) and full width at half maximum (FWHM),

$$N = L/d$$

where, L is the crystallite size (11.79 Å) and d is inter planar distance (3.36 Å). The calculation revealed that the number of graphene layers in the synthesized sample was estimated between 3 and 4. Figure 1(b) demonstrates that WO_3 has crystallized in the monoclinic phase (JCPDS-83-0950), with no other impurity peaks present in the spectrum. The diffraction pattern of WO_3 shows distinct peaks at 23.10, 23.58, 24.33, 28.62, 33.35, 34.11, 41.59, 49.92 and 55.73º, corresponding to the (002), (020), (200), (211), (022), (202), (222), (232), and (142) planes, respectively [14]. The WO_3-FLG NC (Fig. 3(c)) exhibits all the characteristic peaks of both WO_3 and FLG, with modified intensity and slight shift observed due to the formation of the NC.

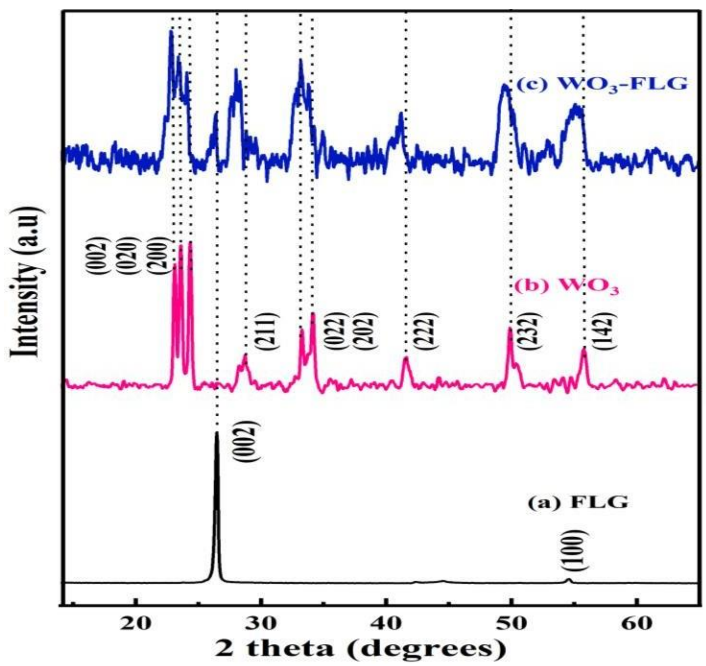

Figure 1: XRD spectra of (a) FLG (b) WO_3 (c) WO_3-FLG

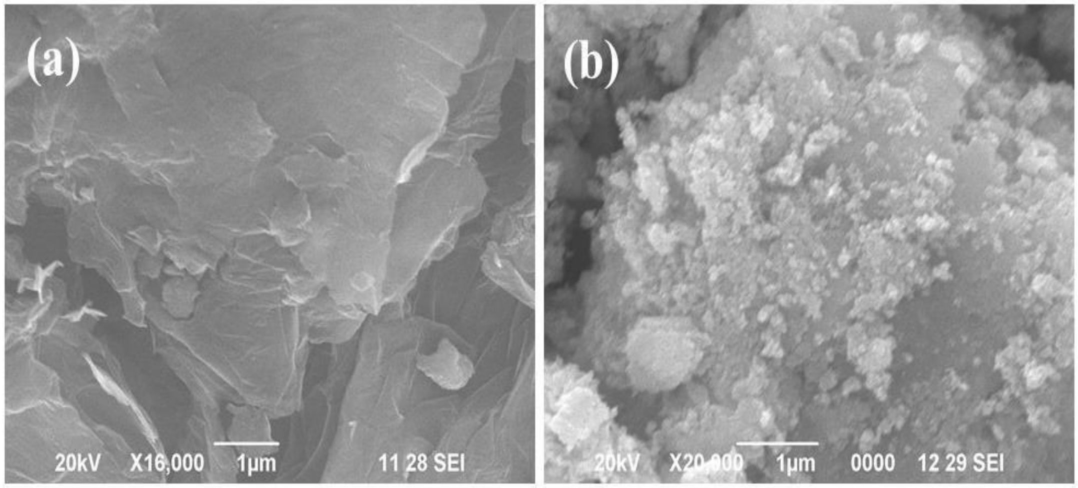

Figure 2: SEM images of (a) FLG and (b) WO_3-FLG

3.2 Scanning Electron Microscopy (SEM)

SEM images of FLG and WO_3-FLG NC are shown in figure 2. The surface of FLG (Fig. 2(a)) shows, folding and wrinkles as reported earlier [23]. In Figure 2(b), the WO_3-FLG NC displays a dense layer of WO_3 NPs anchored onto the FLG surface, indicating a strong interaction between FLG and WO_3 NPs [21].

3.3 Raman spectroscopy

The Raman spectra of FLG, WO_3 and WO_3-FLG NC are shown in Figure 3. FLG spectrum (Fig. 3(a)) shows three prominent peaks around 1340, 1570, and 2700 cm^{-1}, relating to the D, G, and 2D bands. The D band is a marker of structural imperfections in sp^2 bonded carbon materials, arising from out of plane vibrations of carbon atoms. These imperfections can result from missing atoms, structural defects, or impurities in the lattice. The G band is the vibration of sp^2 bonded carbon compounds and relates to the E_{2g} phonon mode, which involves in plane vibrations of carbon atoms in the hexagonal lattice. The 2D band arises from a second order process involving two phonons with opposite momentum. In single layer graphene (SLG), this band is usually sharp and exhibits a Lorentzian shape, along with an I_{2D}/I_G ratio greater than 2, indicating a pristine structure.

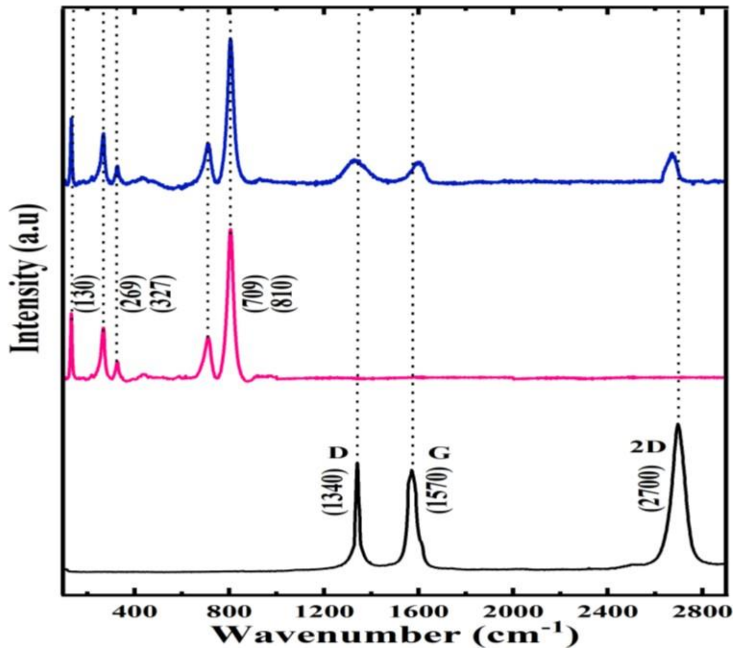

Figure 3: Raman spectra of (a) FLG (b) WO_3 (c) WO_3-FLG

The I_{2D}/I_G ratio can characterize the number of graphene layers. In multilayer graphene, the 2D band broadens and its intensity decreases relative to the G band, reducing the I_{2D}/I_G ratio. As a result, the sharpness, shape, and intensity of the 2D band are used to identify the number of layers in a graphene sheet [24]. In Figure 3(a), the sharp and narrow 2D peak suggests the presence of FLG sheet, which was further confirmed by the Lorentzian multi-peak fitting performed using Origin Pro software, as shown in Figure 4. The FLG sample displays four bands at 2660, 2684, 2701, and 2721 cm^{-1}. The intensity ratio of the G and 2D peaks (I_{2D}/I_G) is 1.44, indicating that few graphene layers are successfully exfoliated from graphite using simple ultra-sonication technique and centrifugation.

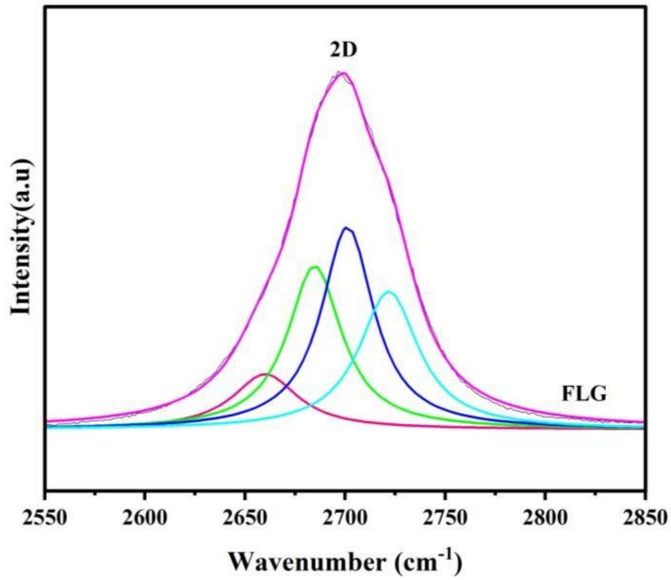

Figure 4: Lorentzian multi-peak fit of 2D peak

The WO_3 sample (Fig. 3(b)) exhibits distinct peaks at 130, 269, 327, 709, and 810 cm^{-1}. The peak at 130 cm^{-1} corresponds to the W-O stretching vibration, while the peaks at 269 and 327 cm^{-1} are attributed to O-W-O stretching modes. Furthermore, the peaks at 709 and 810 cm^{-1} represent O-W-O bending modes. These W-O and O-W-O stretching and bending vibrations clearly indicate the presence of the monoclinic phase WO_3 [25]. The WO_3-FLG NC (Fig. 3(c)) displays all characteristic peaks of both WO_3 and FLG. The I_D/I_G ratio for the FLG and WO_3-FLG NC samples is 0.70 and 1.09, respectively, with a slight shift in the FLG spectrum. This shift and increased intensity ratio proves that FLG inclusion introduces a significant number of defects within the NC.

3.4 Antibacterial activity

Figures 5 and 6 show photographs of petri dishes containing WO_3 and WO_3-FLG NC, tested against S. aureus and E. coli bacteria. The antibacterial activity results for four different concentrations (25, 50, 75, and 100 mL) are presented in Table 1. All the concentrations of WO_3 and WO_3-FLG NC have antibacterial qualities. However, WO_3-FLG NC loading considerably improves antibacterial inactivation, compared to WO_3. Bacterial inactivation was dependent on the four concentrations of WO_3 and WO_3-FLG NC individually. After 24 hours of inhibition proving that FLG significantly improved antibacterial efficacy due to the synergistic effect of WO_3 and FLG.

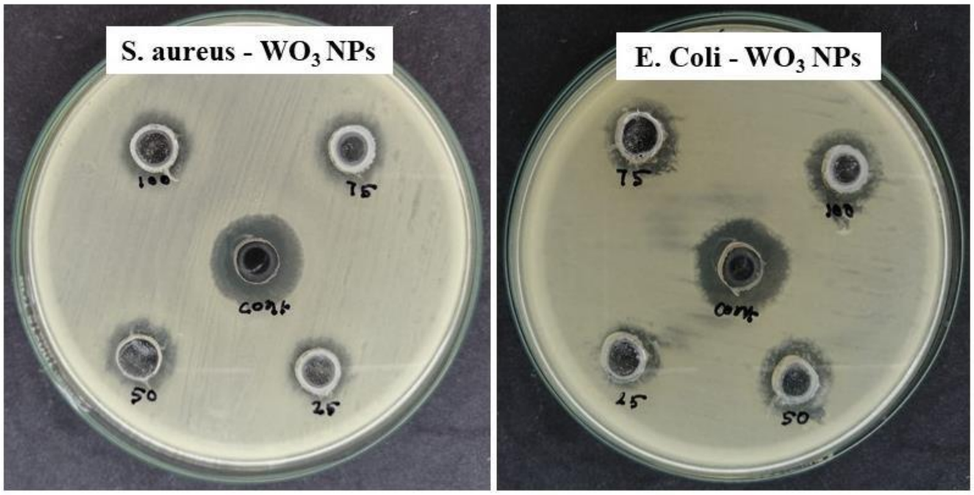

Figure 5: Images of antibacterial activity of WO_3 against S. aureus and E. coli bacteria

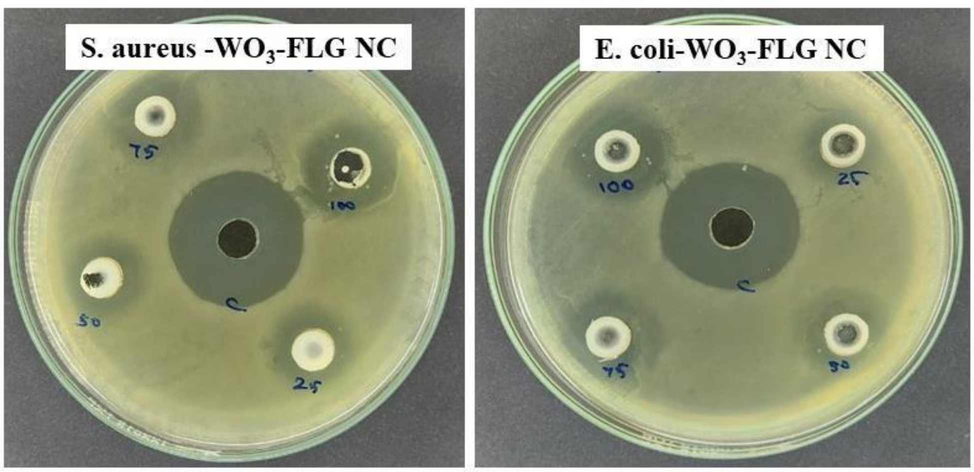

Figure 6: Images of antibacterial activity of WO_3-FLG NC against S. aureus and E. coli bacteria

Graphene based materials can interact with proteins, lipids, DNA, and RNA of bacterial strains, causing electrostatic attraction and inducing membrane stress, leading to cell death or inactivation. Hence, FLG supported WO_3 and improved antibacterial effectiveness. The antibacterial activity of WO_3 and WO_3-GO nanocomposites is attributed to the electrostatic interaction mechanism with S. aureus and E. coli triggered by charge differences. Duan *et al.* [26] reported the inactivation of E. coli and S. aureus bacteria using WO_3 NRs. Muzaffar *et al.* [11] used WO_3-GO NCs to examine killing behaviour against P. aeruginosa and E. coli.

Table 1: Zone of inhibition (mm) for WO_3 and WO_3-FLG NC

Strain	**Zone of inhibition (mm) Concentration (µl)**				
	WO_3 NPs				
	Control	**25**	**50**	**75**	**100**
S. aureus	20	03	04	06	09
E. coli	20	03	05	08	10
	WO_3-FLG NC				
S. aureus	20	06	08	12	14
E. coli	20	08	09	13	15

3.5 Anticancer activity

The cytotoxic activity of WO_3 and WO_3-FLG NC was examined against human breast cancer cells (line MDA-MB-231) using MTT assay is shown in Figure 7. Figure 7(a) display images of MDA-MB-231 cells, while Figures 7(b) and (c) show cytotoxicity images of WO_3 and WO_3-FLG NC, respectively. Figure 8 shows the variation of inhibition of cancer cells treated with WO_3 NPs at different concentrations compared to the control. Figure 9 shows the variation of inhibition of cancer cells treated with WO_3-FLG NC at different concentrations compared to the control. It is found that, cancer cell inhibition increases with increasing concentrations (10-100 µg/ml) of WO_3 and WO_3-FLG NC. The results show that 50% cell inhibition requires 50.62 µg/ml of WO_3, but the same amount of inhibition is attained with 40.75 µg/ml of WO_3-FLG NC. WO_3-FLG NC outperform WO_3 by inhibiting at a lower concentration (IC_{50} = 40.75 µg/ml). A comparable type of assessment was presented by G. Jeevitha *et al.* [7], in which the authors reported the cytotoxicity effect of WO_3 and WO_3-GO NC against human lung cancer cells. J. Kumari *et al.* [27] testified the cytotoxicity effect of WO_3 NPs against human breast cancer cells in the same way.

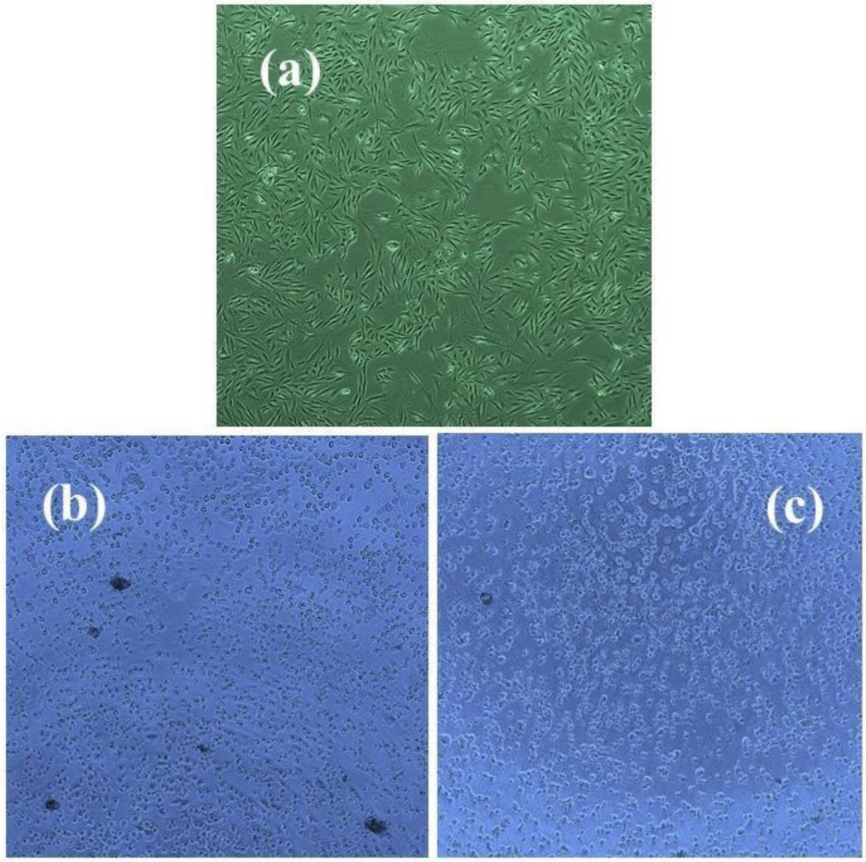

Figure 7: (a) MDA-MB-231 cells and cytotoxicity images of (b) WO_3 and (c) WO_3-FLG NC

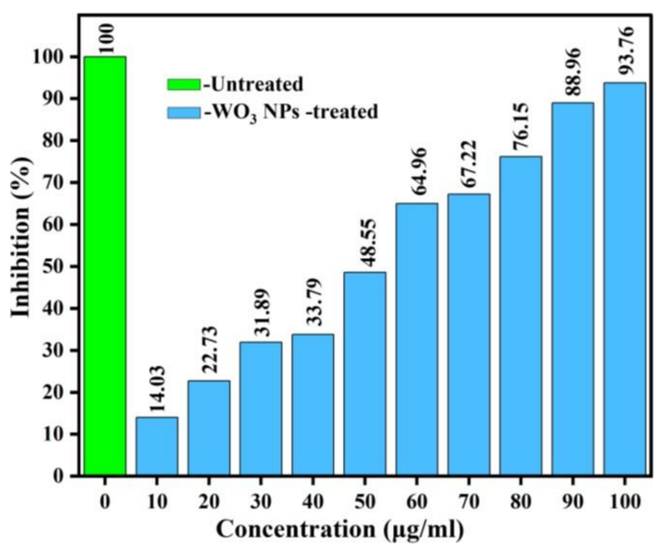

Figure 8: Inhibition of cancer cells treated with WO_3 NPs at different concentrations compared to the control

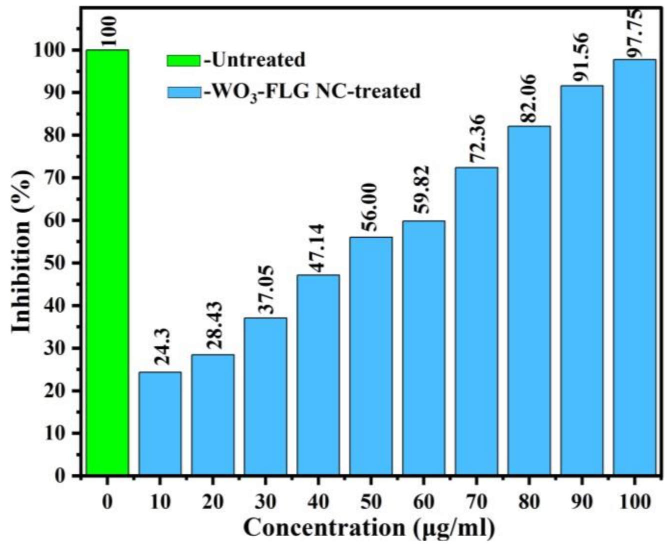

Figure 9: Inhibition of cancer cells treated with WO_3-FLG NC at different concentrations compared to the control

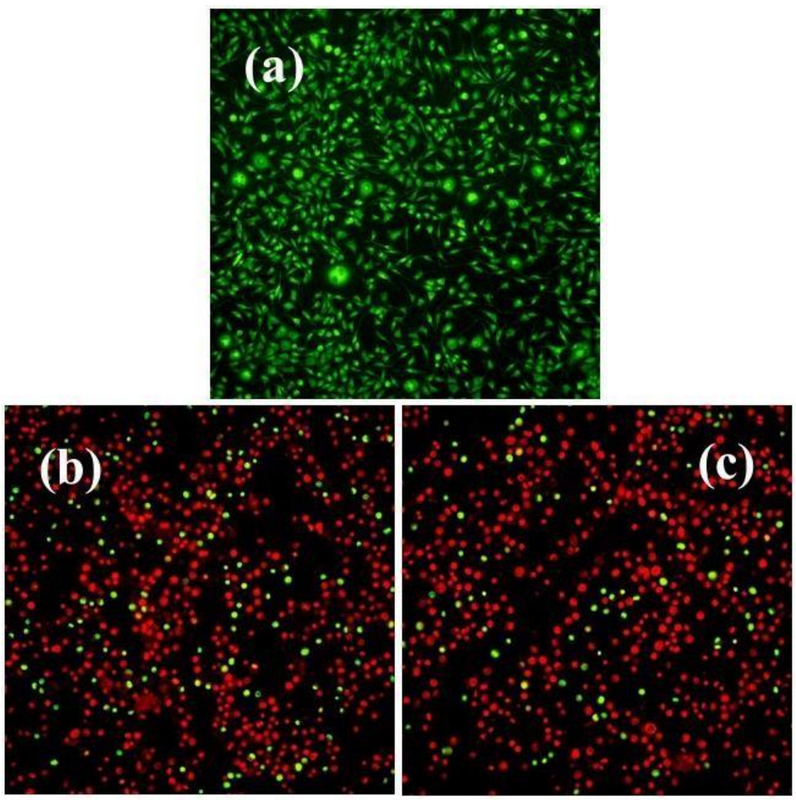

Figure 10: (a) MDA-MB-231 cells and cytotoxicity images of (b) WO_3 and (c) WO_3-FL NC

Apoptosis AO- EB (Acridine Orange/Ethidium Bromide) assay analysis

Figure 10 presents fluorescent pictures obtained from the AO-EB assay, in which the dual AO-EB staining approach was used to study the apoptotic effects of WO_3 and WO_3-FLG NC in MDA-

MB-231 cell lines. In Figure 10(a) (control cells), acridine orange and ethidium bromide staining revealed live cells, and this appeared green in color. MDA-MB-231 cells treated with WO_3 and WO_3-FLG NC at their respective IC_{50} concentrations display major modifications in cell morphology as compared to untreated cells. Figure 10(b) and (c) show that apoptotic cells have tightened, divided, and shifted chromatin, as well as nuclear contraction. Live cells are stained green by AO, other than late apoptotic and necrotic cells show red from EB staining. The WO_3-FLG NC increased cell shrinkage and the quantity of dead cells in the cell lines.

4. Summary

In this work, WO_3 and WO_3-FLG NC are successfully synthesized and characterized for evaluating the structural, morphological, and vibrational properties. The synthesized materials are examined for biological applications. XRD analysis determined that the number of graphene layers in FLG ranged between 3 and 4. Additionally the study infers, WO_3 NPs are of monoclinic crystalline structure and confirming the phase composition of WO_3-FLG NC. SEM analysis revealed the sheet like FLG and dense layers of WO_3 attached on FLG, showing the existence of both the materials. Raman studies confirmed the formation of few layer graphene, along with detailed structural and defect characterization and identified several vibrational modes in WO_3 and WO_3-FLG NC. Both WO_3 and WO_3-FLG NC performs as effective antibacterial agent towards S. aureus as well as E. coli strains. The WO_3 and WO_3-FLG NC showed an IC_{50} concentration against MDA-MB-231 cancer cells at 50.62 and 40.75 μg/ml, respectively. The findings clearly indicated the tested samples may have therapeutic potential against breast cancer cells, depending on the treatment dosage.

5. Acknowledgement

The authors acknowledge, Dr. K. Subramonian, Associate Professor, Department of Botany, The M.D.T. Hindu College, Tirunelveli, Tamilnadu, India for granting laboratory facilities.

6. References

[1] Dutta V, Sharma S, Raizada P, Thakur VK, Khan AAP, Saini V, et al. An overview on WO3based photocatalyst for environmental remediation. J Environ Chem Eng 2021;9. https://doi.org/10.1016/j.jece.2020.105018.

[2] Silambarasan D, Surya VJ, Vasu V, Iyakutti K, Ravindran TR, Jeyanthinath M. Hydrogen adsorption on single walled carbon nanotubes-tungsten trioxide composite. Int J Hydrogen Energy 2017;42:25294–302. https://doi.org/10.1016/j.ijhydene.2017.08.066.

[3] Long H, Zeng W, Zhang H. Synthesis of WO3 and its gas sensing: a review. Journal of Materials Science: Materials in Electronics 2015;26:4698–707. https://doi.org/10.1007/s10854-015-2896-4.

[4] Chang CM, Chiang YC, Cheng MH, Lin SH, Jian W Bin, Chen JT, et al. Fabrication of WO3 electrochromic devices using electro-exploding wire techniques and spray coating. Solar Energy Materials and Solar Cells 2021;223. https://doi.org/10.1016/j.solmat.2021.110960.

[5] Srisitthiratkul C, Yaipimai W, Intasanta V. Environmental Remediation and Interfacial Properties of Nanosilver-Decorated WO_3 Nanofiber sunder Visible Light Source. 2012.

[6] Momai MF, Ookawara S, Alalm MG, Kh El-Etriby H. 2020 Advances in Science and Engineering Technology International Conferences (ASET). 2020.

[7] Jeevitha G, Abhinayaa R, Mangalaraj D, Ponpandian N. Tungsten oxide-graphene oxide (WO3-GO) nanocomposite as an efficient photocatalyst, antibacterial and anticancer agent. Journal of Physics and Chemistry of Solids 2018;116:137–47. https://doi.org/10.1016/j.jpcs.2018.01.021.

[8] Vozniakovskii AA, Smirnova EA, Apraksin R V., Kidalov S V., Voznyakovskii AP. Use of Few-Layer Graphene Synthesized under Conditions of Self-Propagating High-Temperature Synthesis for Supercapacitors Applications. Nanomaterials 2023;13. https://doi.org/10.3390/nano13162368.

[9] Abbas Q, Shinde PA, Abdelkareem MA, Alami AH, Mirzaeian M, Yadav A, et al. Graphene Synthesis Techniques and Environmental Applications. Materials 2022;15. https://doi.org/10.3390/ma15217804.

[10] Rakkesh RA, Durgalakshmi D, Balakumar S. Beyond Chemical Bonding Interaction: An Insight into the Growth Process of 1D ZnO on Few-Layer Graphene for Excellent Photocatalytic and Room Temperature Gas Sensing Applications. ChemistrySelect 2018;3:7302–9. https://doi.org/10.1002/slct.201800987.

[11] Muzaffar T, Khosa RY, Iftikhar U, Obodo RM, Sajjad S, Usman M. Synthesis and Characterization of WO_3/GO Nanocomposites for Antimicrobial Properties. J Clust Sci 2022;33:1987–96. https://doi.org/10.1007/s10876-021-02116-2.

[12] Ahmed B, Ojha AK, Hirsch F, Fischer I, Patrice D, Materny A. Tailoring of enhanced interfacial polarization in WO_3 nanorods grown over reduced graphene oxide synthesized by a one-step hydrothermal method. RSC Adv 2017;7:13985–96. https://doi.org/10.1039/c7ra00730b.

[13] Alaizeri ZAM, Alhadlaq HA, Aldawood S, Akhtar MJ, Ahamed M. Bi2O3-Doped WO_3 Nanoparticles Decorated on rGO Sheets: Simple Synthesis, Characterization, Photocatalytic

Performance, and Selective Cytotoxicity toward Human Cancer Cells. ACS Omega 2023;8:25020–33. https://doi.org/10.1021/acsomega.3c01644.

[14] Mohan L, Avani A V., Kathirvel P, Marnadu R, Packiaraj R, Joshua JR, et al. Investigation on structural, morphological and electrochemical properties of Mn doped WO3 nanoparticles synthesized by co-precipitation method for supercapacitor applications. J Alloys Compd 2021;882. https://doi.org/10.1016/j.jallcom.2021.160670.

[15] Gayathri S, Jayabal P, Kottaisamy M, Ramakrishnan V. Synthesis of few layer graphene by direct exfoliation of graphite and a Raman spectroscopic study. AIP Adv 2014;4. https://doi.org/10.1063/1.4866595.

[16] Silambarasan D, Surya VJ, Vasu V, Iyakutti K. Single walled carbon nanotube-metal oxide nanocomposites for reversible and reproducible storage of hydrogen. ACS Appl Mater Interfaces 2013;5:11419–26. https://doi.org/10.1021/am403662t.

[17] Balouiri M, Sadiki M, Ibnsouda SK. Methods for in vitro evaluating antimicrobial activity: A review. J Pharm Anal 2016;6:71–9. https://doi.org/10.1016/j.jpha.2015.11.005.

[18] Mirzayans R, Andrais B, Murray D. Viability assessment following anticancer treatment requires single-cell visualization. Cancers (Basel) 2018;10. https://doi.org/10.3390/cancers10080255.

[19] Ribble D, Goldstein NB, Norris DA, Shellman YG. A simple technique for quantifying apoptosis in 96-well plates. BMC Biotechnol 2005;5. https://doi.org/10.1186/1472-6750-5-12.

[20] Vinayan BP, Schwarzburger NI, Fichtner M. Synthesis of a nitrogen rich (2D-1D) hybrid carbon nanomaterial using a MnO2 nanorod template for high performance Li-ion battery applications. J Mater Chem A Mater 2015;3:6810–8. https://doi.org/10.1039/c4ta05642f.

[21] Rakkesh RA, Durgalakshmi D, Balakumar S. Beyond Chemical Bonding Interaction: An Insight into the Growth Process of 1D ZnO on Few-Layer Graphene for Excellent Photocatalytic and Room Temperature Gas Sensing Applications. ChemistrySelect 2018;3:7302–9. https://doi.org/10.1002/slct.201800987.

[22] Patterson AL. The Scherrer Formula for I-Ray Particle Size Determination. vol. 56. 1939.

[23] Bajpai R, Roy S, Jain L, Kulshrestha N, Hazra KS, Misra DS. Facile one-step transfer process of graphene. Nanotechnology 2011;22. https://doi.org/10.1088/0957-4484/22/22/225606.

[24] Nazarov AN, Gordienko SO, Lytvyn PM, Strelchuk V V., Nikolenko AS, Vasin A V., et al. Characterization of graphene layers by Kelvin probe force microscopy and micro-Raman

spectroscopy. Physica Status Solidi (C) Current Topics in Solid State Physics 2013;10:1172–5. https://doi.org/10.1002/pssc.201200918.

[25] Bhargava R, Khan S. Fabrication of WO_3–reduced graphene oxide (WO_3–G) nanocomposite for enhanced optical and electrical properties. Journal of Materials Science: Materials in Electronics 2020;31:8370–84. https://doi.org/10.1007/s10854-020-03372-0.

[26] Duan G, Chen L, Jing Z, De Luna P, Wen L, Zhang L, et al. Robust Antibacterial Activity of Tungsten Oxide (WO3-x) Nanodots. Chem Res Toxicol 2019;32:1357–66. https://doi.org/10.1021/acs.chemrestox.8b00399.

[27] Kumari J, Mangala P. Enhanced Anticarcinogenic and Antimicrobial Response of Synthesized Tungsten Oxide Nanoparticles. Journal of Scientific Research 2023;15:141–57. https://doi.org/10.3329/jsr.v15i1.58211.